This is an *Accepted Manuscript*, which has been through the Royal Society of Chemistry peer review process and has been accepted for publication.

Accepted Manuscripts are published online shortly after acceptance, before technical editing, formatting and proof reading. Using this free service, authors can make their results available to the community, in citable form, before we publish the edited article. We will replace this *Accepted Manuscript* with the edited and formatted *Advance Article* as soon as it is available.

You can find more information about *Accepted Manuscripts* in the **Information for Authors**.

Please note that technical editing may introduce minor changes to the text and/or graphics, which may alter content. The journal's standard **Terms & Conditions** and the **Ethical guidelines** still apply. In no event shall the Royal Society of Chemistry be held responsible for any errors or omissions in this *Accepted Manuscript* or any consequences arising from the use of any information it contains.

Journal Name

ARTICLE TYPE

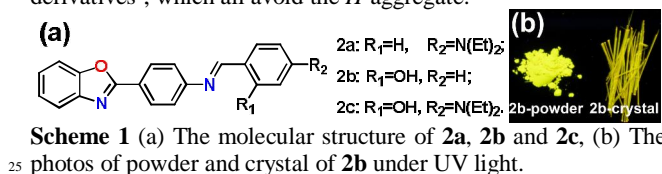# Novel highly emissive *H*-aggregates with aggregate fluorescence change in phenylbenzoxazole-based system

Lianke Wang, Yanfang Shen, Weinan Xu, Qiuju Zhu, Jieying Wu, Yupeng Tian, Hongping Zhou*

Fibrous nanoaggregates of a new benzoxazole-based derivative have been reported. It exhibit not only *H*-aggregates but also highly yellow fluorescence, which is different from the traditional understanding of H-aggregates.

10 Designing novel chromophores with excellent optical properties in the condensed state have been a popular research for their potential applications in organic light emitting diodes (OLEDs)[1], fluorescent sensors[2] and *et al*. The restriction of intramolecular rotation (RIR) or planarization and *J*-aggregation reported by
15 Tang[3] and Park[4] are in favor of enhancing emission. The frequently reported aggregation-caused quenching fluorescence (ACQ)[5] in *H*-aggregates has greatly limited their potential applications. At present, various excellent chromophores with aggregation-induced emission[3] or enhanced emission[4] (AIE/AIEE)
20 properties have been developed by many research groups, such as tetraphenylethene[6], cyanostilbene[7] and 9, 10-distyrylanthracene derivatives[8], which all avoid the *H*-aggregate.

Scheme 1 (a) The molecular structure of **2a**, **2b** and **2c**, (b) The
25 photos of powder and crystal of **2b** under UV light.

Considering interesting fluorescence properties of benzoxazole, we utilized benzoxazole as building blocks and changed the terminal substituents to build new phenylbenzoxazole-based chromophores. The structures of targeted molecules are shown in
30 **Scheme S1**. In this communication, we reported the highly emissive *H*-aggregate **2b** and the unique AIEE phenomenon with large red shifts and remarkable color change. Thermogravimetric analysis (TGA) and differential scanning calorimetry (DSC) results indicate that all compounds hold high melting points with
35 T_m at 139.9, 235.8 and 201.9 $^{\circ}$C (Tab 1), respectively, and high thermal stability with T_d at 294, 273 and 294 $^{\circ}$C (Tab 1), respectively.

We initially investigated the absorption and fluorescence spectra of **2a-2c** (10 μM) in various polarity solvents (Tab S1 and
40 Fig. S1, ESI†). The absorption and fluorescence spectra of **2a-2c** demonstrate quite similar maxima in the different solvents meaning the slight solvent-dependence. The targeted molecules show strong absorption bands at 388, 327 and 414 nm, respectively, and emission maxima ($_{em}$) at 499, 389 and 495nm,
45 respectively. The weak absorption peaks at 300-320 nm that are mainly attributed to - * electronic transitions derived from the benzoxazolyl-benzene unit[9]. The molar extinction coefficient values also are in agreement with - * transitions[10]. Theoretical calculations are liable method for qualitative indication of the
50 absorption properties.[11] We calculated frontier molecular orbital based on the molecular conformations in the crystal structures. Further details are given in the ESI and the results are in good agreement with the experimental absorption spectra. All data indicate that the introduction of diethylamino groups can change
55 the -conjugated degree of benzoxazolyl compounds.

Tab 1.Optical properties of the targeted molecules.

Compd	$_{abs}$/nm	$_{em}$/nm				T_m(°C)	T_d(°C)
		Pure	Mixed	Powder	Crystal		
2a	388	499	518	552	593	139.9	294
2b	327	389	542	581	588	235.8	273
2c	414	495	564	564	564	201.9	294

$_{abs}$ = the maxima absorption peak, $_{em}$ = the maxima emission peak, in dilute ethanol solution (10^{-5} mol L^{-1}), Pure = the pure ethanol solution, Mixed = the mixed water/ethanol solution with f_w =0.90, T_d = temperature for 5% weight loss, T_m = melting temperature recorded by differential scanning calorimeter.
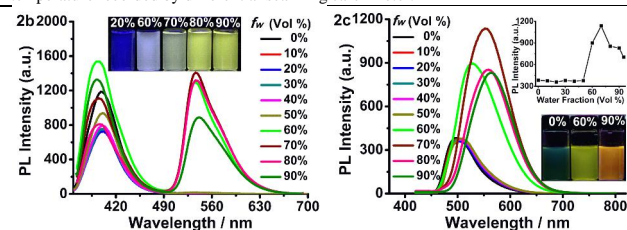

Fig 1. The fluorescence spectra of **2b** and **2c** in water/ethanol mixtures with different water fraction (f_w). The inset depicts the
60 changes of PL peak intensity with different f_w. Photos of **2b** and **2c** in the water/ethanol mixtures with different f_w are taken under UV light. Concentration: 50 μM.

2a-2c molecules exhibit weak green, blue and cyan emission in diluted ethanol solution under UV light (The inset in Fig S2, ESI†
65 and Fig 1), respectively. Firstly, the fluorescence intensity of **2a** is almost linearly increasing step by step with the increasing of water fraction, accompanying with red-shift in the $_{em}$ values. The light emission reaches its maximum value when f_w = 70%, which is 6.4-fold higher than that in pure ethanol solution. **2b** plays
70 different fluorescent behaviors in ethanol/water solutions with different f_w values. Upon addition of water, the emission intensity and wavelength show a slight decrease and red shift, respectively. When f_w 60% (Fig 1), the yellow emission band centred at 542 nm rapidly turn on. The inset photos (Fig 1) taken under UV light
75 describe the color change and we can clearly see that the blue the solution vividly transfer into yellow. In addition, **2c** also exhibits

the changes of the emission from cyan to orange with red-shift of 70 nm after addition of different amount of water. The fluorescence intensity remain unchanged until the f_w is increased to 60%, the solutions emit bright yellow light with $_{em}$ at 528nm. The emission intensity reaches its maximum value at $f_w = 70\%$ and the $_{em}$ red shift to 564 nm when $f_w = 90\%$. Such ratiometric fluorescence changes with a large red-shift of 150 and 70 nm for **2b** and **2c** in benzoxazole-based compounds has so far never been reported, not to mention the impressive color changes. These unique AIEE behaviors are very significant in the field of fluorescent probes. The absorption spectra of **2a** and **2c** show a slight bathochromic shift and level-off tail in the long-wavelength regions. The tail is caused by the Mie scattering effect[6], which suggests the formation of nanoaggregates. While the absorption spectrum of **2b** exhibits a slight blue-shift and arises a few new absorption peaks between 370 and 420 nm when f_w 60%, which indicate the formation of new species.

To gain further insight into the unique morphology of the nanoaggregates of these benzoxazole-based compounds in the mixture system, the mixture solutions was subjected to the scanning electron microscopy (SEM) observation. As can be seen from the photos shown in Fig 2a and Fig S3, three benzoxazole-based compounds aggregate to form three different shapes in the mixture system. A large number of block nanoparticles of **2a** formed immediately in the mixture of ethanol/water with $f_w = 80\%$ (Fig. S3a, ESI†). It is noteworthy that **2b** molecules aggregate to form entangled three dimensional networks consisting of the interconnected fibrous nanoaggregates, which has so far never been reported in benzoxazole-based compounds (Fig. 2a).[12] For **2c**, it aggregates into the rice-like shape nanoparticles in ethanol/water mixtures (Fig S3c, ESI†). These above mentioned images must be responsible for the observed enhanced emission and the impressive color changes.
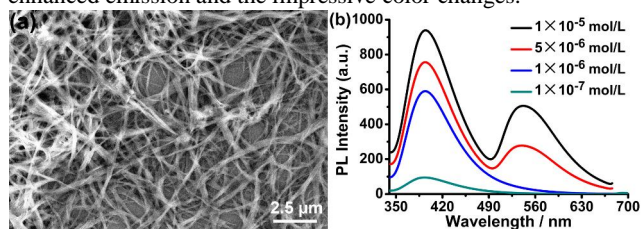

Fig 2. (a). The SEM images of the nanoaggregates of **2b** prepared in ethanol/water (2:8) mixtures at concentrations of 50 μM. (b). The PL spectrum of **2b** in different concentrations with $f_w = 80\%$.

We also comparatively investigated their emissions in the different state. Their normalized fluorescence spectra are shown in Fig S4 and relative emission wavelength are shown in Tab 1. All compounds exhibit the minimum emission wavelength in the pure ethanol solution and the maximum emission wavelength in the crystal state. **2a** and **2b** show the same trend: $_{em/Pure} < _{em/Mixed} < _{em/Powder} < _{em/Crystal}$, while **2c** displays $_{em/Pure} < _{em/Mixed}$ $_{em/Powder}$ $_{em/Crystal}$.

According to some other AIE/AIEE-active system, the reasons for these unique fluorescent behaviors can be tentatively ascribed to the different molecular conformations and packing modes in the different states[13]. In the pure ethanol solution, these compounds molecules are molecularly isolated without any interactions between the adjacent molecules, and the molecules have highly twisted conformations due to the intramolecular

steric hindrance, which leads to the minimum $_{em}$. The molecules of **2a-2c** in the crystal state are arranged so regularly that the rotatable single bonds are locked due to the multiply physical intermolecular interactions (see the following crystal discussions). These increase the molecular planarity and strengthen the - conjugated systems, which contribute to the maximum $_{em}$. While the powder states have less regularity compared with that in the crystal states. In condensed solution, **2a** shows the common feature just like some other AIE/AIEE-active systems, **2b** may form multimers in the mixture with high water content. The emission wavelength of **2c** in the mixed solution is close to that in the powder and the crystal state, suggesting that they originate from the same emitting species with similar molecular conformation and interactions.

To obtain a better understanding of the enhanced emission and impressive color change of **2a-2c**, we investigated their crystal structures. The single crystals were obtained by slow evaporation from ethanol, CH_2Cl_2/ethanol and CH_2Cl_2/CH_3CN solution, respectively and their crystallographic data are summarized in Tab S2.
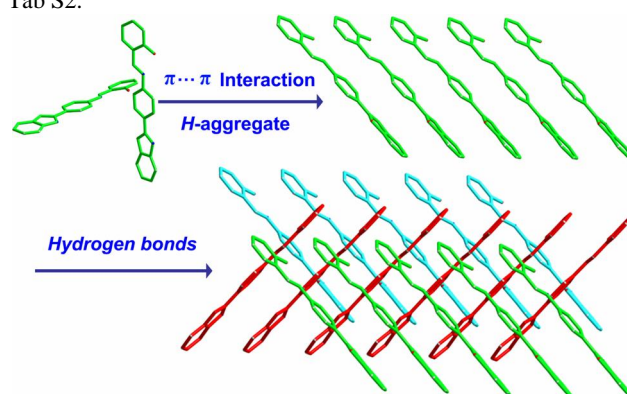

Fig 3. Formation scheme of two dimensional expanded cross packing layer structure of the **2b** molecules. All the hydrogen atoms are omitted for clarity.

As shown in Fig S5, due to the existences of intramolecular hydrogen bonds, they all have a better planarity. The ORTEP diagram with atom numbering and high dimensional structures of **2a** is shown in Fig S6. The adjacent three molecules are cross-linked into one dimensional band in face-to-edge way *via* multiple C-H··· interactions ($d = 2.743, 2.823, 2.964$ and 2.905Å) and C-H···N hydrogen bonds ($d = 2.780$ and 2.747 Å). Furthermore, the more molecules are interconnected by above-mentioned intermolecular interactions to form two dimensional layer structures. The molecular structure of **2b** in the crystal state is nearly coplanar (Fig S7, ESI†). We can clearly see from Fig S7c that the two molecules are initially cross stacked in edge-to-edge type to form an L-shaped dimmer through C-H···O hydrogen bonds between the hydroxystyryl hydrogen atoms and the hydroxy oxygen atom, with the distance measured at 2.716 and 2.680 Å, respectively. As shown in Fig S7b, two **2b** molecules are slip-stacking together in face-to-face type to from *H*-aggregates through ··· stacking interactions with the distance measured at 3.477 Å. The two dimmers are then connected with each other in middle-to-middle way to form #-shaped tetramer through C-H···N ($d = 2.564$ Å) and C-H···O ($d = 2.668$ Å) hydrogen bonds between the hydrogen atoms of the benzoxazolyl and phenyl groups of one molecule and the nitrogen

and oxygen atoms of the benzoxazolyl group of the adjacent molecule. The #-aggregations are further expanded to form a two dimensional multimer crossing layer structure by above-mentioned type of hydrogen bonds and ··· stacking interactions. The formation scheme of the two dimensional expanded cross packing layer structure is shown in Fig 3. For **2c,** its crystal structures are similar to that of **2a**. Fig S9b shows all intermolecular interactions on one molecule, including C-H··· (*d* = 2.735, 2.844 and 2.852 Å), C-O··· (*d* = 3.010 Å) and C-H···N (*d* = 2.847 and 2.699 Å) interactions. **2c** molecules are linked into two dimensional bands *via* the above intermolecular interactions (Fig. S9c, ESI†). Furthermore, these bands structures are connected in head-to-head way to form a three dimensional W-shaped stacking structure by another type of hydrogen bonds between the nitrogen atoms on the oxazolyl rings and the hydrogen atoms of phenyl rings, with the distance measured at 2.796 Å.

According to the crystal structures, the obvious enhanced emission and unique color change can be well explained by these existing multiply interactions. Under the synergetic effect of intra- and intermolecular interactions, intramolecular motions are locked and the molecular conformations are more rigid and planar. Thus, the physical restriction of intramolecular motions and aggregation-induced planarization induced by the molecular aggregation can be considered as the mechanisms of the enhanced emission phenomena of **2a** and **2c**. For **2b**, it is obvious that **2b** molecules have better planarity and aggregate to form multimer in face-to-face type according to its crystal structure. In general, the formations of *H*-aggregate where molecules are aligned parallel to each other with strong intermolecular interactions are characterized by blue-shifted absorption bands, which tend to induce the nonradiative deactivation process.[14] The absorption bands and the crystal structures all prove that **2b** molecules aggregates to form *H*-aggregates. The formation of multimer shows obvious concentration-dependence. When the concentration of **2b** is lower than 1μM in the ethanol/water (2:8) mixtures, the yellow emission at 542 nm disappeared (Fig 2b and Fig. S13, ESI†), which indicate the absence of the special emissive species that show yellow emission. Thus, we can speculate that the emission in yellow region is attributed to the emission of *H*-aggregates, which is quite different from the traditional understanding of *H*-aggregates.

Generally, high radiative rates can efficiently enhance emission, while the active exciton migration is detrimental to emission.[15] Whether the emission quenches or strengthens is determined by the competition between the two opposite factors. Obviously, the positive effect is dominant in the emission process of **2b**. It is very likely that the specific slip-stacking and the dimmer formed by multiple intermolecular hydrogen bonds play essential roles in its high emission, which effectively slow down exciton motion, turn on radiative decay channel and avoid strong *H*-type coupling to some extent, thus *H*-aggregates of **2b** exhibit high emission.

Considering the color changes in solution and nanoaggregates, the application of **2b** nanoaggregates to detect highly volatile organic solvents was investigated on thin-layer chromatography plates (Fig. S12, ESI†). Under the 365 nm of UV light at room temperature, **2b** nanoaggregates show bright yellow fluorescence which turn into blue in the atmosphere of dichloromethane vapour. The color can be recovered after the vapour is removed. Such fluorescence switches indicate that **2b** exhibits different states in different condition. Similar fluorescence change of **2b** can also be observed for other solvents, such as tetrahydrofuran and chloroform. Thus, the fluorescence color changes can be used in detecting highly volatile organic solvents because it can be distinguished easily by eye.

Conclusions

In conclusion, we have revealed enhanced emission with large red shifts and color change of a novel benzoxazole-based derivative. In contrast to the general observation that *H*-aggregates formation quenches the light emissions of chromophores, **2b** exhibit *H*-type aggregates and efficient emission in the aggregate state. The specific slip-stacking and the dimmer formed by multiple intermolecular interactions avoid strong *H*-type coupling and are responsible for highly emissive *H*-type aggregates. The response to volatile organic solvents with blue/yellow fluorescent switching was also demonstrated. **2a** and **2c** show the common AIEE feature. The unique enhanced emission with color changes and efficient emission is suitable for fluorescent probes and OLEDS and also provide new ideas for emissive chromophores.

Notes and references

[a] College of Chemistry and Chemical Engineering, Key Laboratory of Functional Inorganic Materials Chemistry of Anhui Province, Anhui University, Hefei 230601, P. R. China. Fax: +86-551-63861259; Tel: +86-551-63861259; E-mail: zhpzhp@263.net

† Electronic Supplementary Information (ESI) available: Synthesis, characterization, spectra, SEM images and theoretical calculations. See DOI: 10.1039/b000000x/

‡ CCDC number: 994632-994634.

1   (*a*) Z. J. Zhao, J. W. Y. Lam and B. Z. Tang, *J. Mater. Chem.*, 2012, **22**, 23726-23740. (*b*) X. H. Zhu, J. B. Peng, Y. Cao and J. Roncail, *Chem. Sov. Rev.*, 2011, **40**, 3509-3524. (*c*) D. Li, H. Y. Zhang and Y. Wang, *Chem. Sov. Rev.*, 2013, **42**, 8416-8433. (*d*) Y. Zhao, L. Duan, D. Q. Zhang, G. F. Dong, J. Qiao, L. D. Wang and Y. Qiu, *ACS Appl. Mater. Interfaces*, 2014, **6**, 4570-4577.

2   (*a*) C. W. T. Leung, Y. N. Hong, S. J. Chen, E. G. Zhao, J. W. T. Lam and B. Z. Tang, *J. Am. Chem. Soc.*, 2013, **135**, 62-65. (*b*) Z. K. Wang, S. J. Chen, J. W. Y. Lam, W. Qin, R. T. K. Kwok, N. Xie, Q. L. Hu, and B. Z. Tang, *J. Am. Chem. Soc.*, 2013, **135**, 8238-8245. (*c*) H. B. Shi, R. T. K. Kwok, J. Z. Liu, B. G. Xing, B. Z. Tang and B. Liu, *J. Am. Chem. Soc.*, 2012, **134**, 17972-17981.(*d*) D. Ding, K. Li and B. Z. Tang, *Acc. Chem. Res.*, 2013, **46**, 2441-2453.

3 J. D. Luo, Z. L. Xie, J. W. Y. Lam, L. Cheng, H. Y. Chen, C. F. Qin, H. S. Kwok, X. W. Zhan, Y. Q. Liu, D. B. Zhu and B. Z. Tang, *Chem. Commun.*, 2001, 1740-1741.

4 B. K. An, S. K. Kwon, S. D. Jung and S. Y. Park, *J. Am. Chem. Soc.*, 2002, **124**, 14410-14415.

5 J. B. Birks, Wiley: London, UK, 1970.

6 (*a*) Y. Q. Dong, J. W. Y. Lam, A. J. Qin, J. Z. Liu, Z. Li, B. Z. Tang, J. X. Sun, H. S. Kwok, *Appl. Phys. Lett.*, 2007, **91**, 011111. (*b*) C. W. T. Leung, Y. N. Hong, S. J. Chen, E. G. Zhao, J. W. Y. Lam and B. Z. Tang, *J. Am. Chem. Soc.*, 2013, **135**, 62-65. (*c*) Y. Y. Yuan, R. T. K. Kwok, G. X. Feng, J. Liang, J. L. Geng, B. Z. Tang and B. Liu, *Chem. Commun.*, 2014, **50**, 295-297.

7 (*a*) B. K. An, J. Gierschner and S. Y. Park, *Acc. Chem. Res.*, 2012, **45**, 544-554. (*b*) X. Q. Zhang, X. Y. Zhang, B. Yang, Y. L. Zhang and Y. Wei, *ACS Appl. Mater. Interfaces*, 2014, **6**, 3600-3606.

8 (*a*) X. Q. Zhang, Z. G. Chi, B. J. Xu, L. Jiang, X. Zhou, Y. Zhang, S. W. Liu and J. R. Xu, *Chem. Commun.*, 2012, **48**, 10895-10897. (*b*) M. Zheng, D. T. Zhang, M. X. Sun, Y. P. Li, S. F. Xue and W. J. Yang, *J. Mater. Chem. C*, 2014, **2**, 1913-1920. (*c*) X. Q. Zhang, Z. Y. Ma, Y. Yang, X. Y. Zhang, Z. G. Chi, S. W. Liu, J. R. Xu, X. R. Jia and Y. Wei, *Tetrahedron*, 2014, **70**, 924-929.

9 L. K. Wang, Z. Zheng, Z. P. Yu, J. Zheng, M. Fang, J. Y. Wu, Y. P. Tian and H. P. Zhou, *J. Mater. Chem. C*, 2013, **1**, 6952-6959.

10 F. S. Santos, T. M. H. Costa, V. Stefani, P. F. B. Gonalves, R. R. Descalzo, E. V. Benvenutti and F. S. Rodembusch, *J. Phys. Chem. A*, 2011, **115**, 13390-13398.

11 X. Y. Shen, Y. J. Wang, E. G. Zhao, W. Z. Yuan, Y. Liu, P. Lu, A. J. Qin, Y. G. Ma, J. Z. Sun and B. Z. Tang, *J. Phys. Chem. C*, 2013, **117**, 7334-7347.

12 (*a*) Y. Qian, M. M. Cai, X. H. Zhou, Z. Q. Gao, X. P. Wang, Y. Z. Zhao, X. H. Yan, W. Wei, L. H. Xie and W. Huang, *J. Phys. Chem. C*, 2012, **116**, 12187-12195. (*b*) X. P. Li, Y. Qian, S. Q. Wang, S. Y. Li and G. Q. Yang, *J. Phys. Chem. C*, 2009, **113**, 3862-3868.

13 Z. P. Yu, Y. Y. Duan, L. H. Cheng, Z. L. Han, Z. Zheng, H. P. Zhou, J. Y. Wu and Y. P. Tian, *J. Mater. Chem.*, 2012, **22**, 16927-16932.

14 Y. N. Hong, J. W. Y. Lam and B. Z. Tang, *Chem. Soc. Rev.*, 2011, **40**, 5361-5388.

15 (*a*) D. Oelkrug, A. Tompert, J. Gierschner, H. J. Egelhaaf, M. Hanack, M. Hohloch, E. Steinhuber, *J. Phys. Chem. B*, 1998, **102**, 1902-1907. (*b*) K. H. Schweikart, M. Hohloch, E. Steinhuber, M. Hanack, L. Lüer, J. Gierschner, H. J. Egelhaaf, D. Oelkrug, *Synth. Met.*, 2001, **121**, 1641-1642. (*c*) J. Gierschner, L. Lüer, B. Milián-Medina, D. Oelkrug, H. J. Egelhaaf, *J. Phys. Chem. Lett.*, 2013, **4**, 2686-2697.